# Charge distribution and screening in layered graphene systems

F. Guinea
*Instituto de Ciencia de Materiales de Madrid, CSIC, Cantoblanco, 28049 Madrid, Spain*
(Received 7 November 2006; revised manuscript received 20 March 2007; published 21 June 2007)

The charge distribution induced by external fields in finite stacks of graphene planes, or in semi-infinite graphite is considered. The interlayer electronic hybridization is described by a nearest-neighbor hopping term, and the charge induced by the self-consistent electrostatic potential is calculated within the linear response theory (random phase approximation). The screening properties are determined by contributions from interband and intraband electronic transitions. In neutral systems, only interband transitions contribute to the charge polarizability, leading to insulatinglike screening properties, and to oscillations in the induced charge, with a period equal to the interlayer spacing. In doped systems, we find a screening length that is equivalent to two-to-three graphene layers, superimposed to significant charge oscillations.

DOI: 10.1103/PhysRevB.75.235433 PACS number(s): 73.22.−f, 73.21.Ac, 73.20.−r

## I. INTRODUCTION

Electronically charged systems made up of a few graphene layers are being intensively studied,[1–8] as well as the effects of charge accumulation on the surface of bulk graphite.[9,10] The transport properties of multilayered samples depend on the distribution of carriers among the graphene layers. The hybridization between layers does not favor interlayer hopping, as the low-energy bands are mostly localized on atoms which are not coupled to the neighboring layers.[11] Hence, in a first approximation, transport in the direction parallel to the layers can be analyzed as arising from independent layers attached in parallel to the leads. It is well known that the transport properties of a single graphene layer depend on its carrier density.[12] Hence, a knowledge of the charge distribution in multilayered samples is needed in order to study further their transport properties.

It is known that screening in a single graphene layer shows anomalous properties, due to the vanishing of the density of states at the Fermi level in neutral graphene.[13,14] A stack of graphene planes where electrons are confined to each layer also shows unusual screening properties.[15] In addition, defects and edges can lead to self-doping effects in a single graphene layer.[16]

The screening properties of bulk graphite were initially investigated by describing the system as a stack of two-dimensional electron fluids electrostaticaslly coupled.[17] The electronic hybridization between layers was not included in the model, and the carriers within each layer were described as filling a small electron pocket parametrized by a finite effective mass.

In this work we extend the model in Ref. 17 by (i) including the interlayer hopping, described by a term which hybridizes $\pi$ orbitals at carbon atoms at nearest-neighbor positions in contiguous layers,[18,19] and (ii) describing the electronic structure within each layer by the massless Dirac equation. As it will be discussed below, these modifications change significantly the screening properties in graphene multilayered samples.

The charge distribution in systems under an applied field must be calculated self-consistently. Such a calculation, using the interlayer hopping model described above, has been carried out for a graphene bilayer.[20] In the following, we calculate the charge distribution in graphene stacks of arbitrary width, and in semi-infinite graphite. We calculate the electrostatic potential self-consistently, and assume that the induced charge can be obtained using linear response theory. These assumptions amount to the random phase approximation, applied to the model mentioned earlier. A similar calculation for a bilayer can be found in Ref. 20 and it is in reasonable agreement with more involved numerical calculations.

We use, as a starting point, the calculations of the unperturbed electronic structure of finite graphene stacks, and semi-infinite graphite, reported in Ref. 18. We do not study the effects of other interlayer hoppings, disorder, or other effects related to interactions. We also do not consider deviations from Bernal stacking, $\{1212\cdots\}$, which can alter the electronic structure at the Fermi level.[18]

The following section presents the model to be studied. We discuss the screening in semi-infinite graphite, and we analyze a finite graphene stack. Section IV presents the main conclusions of our work. It also contains a discussion of the limits of validity of the results presented here, and their relation to previous work.

## II. THE MODEL

### A. Electrostatic effects

We analyze the charge distribution at the surface layers of a system with many graphene layers coupled electrostatically to an external gate. The system is schematically shown in Fig. 1. A potential $V$ is applied between the gate and the graphene stack. An electric field, $\mathcal{E}=V/l$, where $l$ is the distance between the gate and the stack. This setup resembles the situation found in samples obtained by exfoliating graphite which are doped by means of a metallic gate.[3] In samples grown epitaxially on a SiC substrate,[1] the difference in work functions between the graphene layers and the substrate leads to some charge transfer, and to the appearance of electric fields at the interface between the substrate and the graphene layers.

The electric potential beyond the gate is assumed to be zero, and the voltage at the gate is $-V$. Using Gauss law we

 

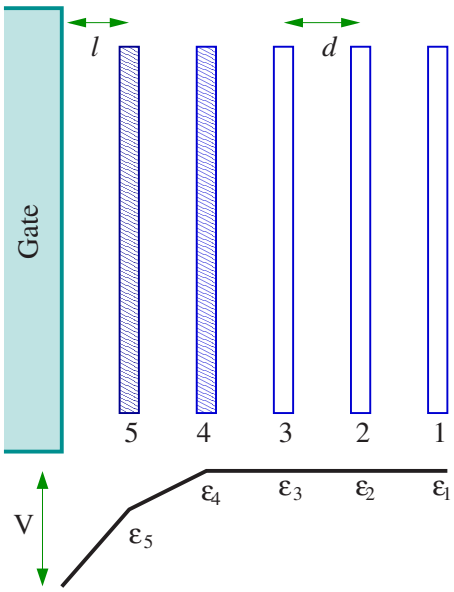


FIG. 1. (Color online) Sketch of the system studied in the text. The two layers closest to the gate are charged, and lead to the electrostatic potential shown in the lower part.

can write the total charge density per unit area in the stack, $n$ as $en=4\pi\mathcal{E}$. This charge is distributed among the layers, $n_1,n_2,n_3,\ldots$ where label 1 stands for the outermost layer. The electric field in the region between layers 1 and 2 is $\mathcal{E}_{1-2}=4\pi en_1/d$, where $d$ is the interlayer distance. This field determines the potential in layer 2. Extrapolating this procedure to all layers, we find that the electrostatic potential in layer $i$ satisfies

$$\epsilon_i = \epsilon_{i-1} + 4\pi e^2 d \sum_{k=1}^{i-1} n_k \tag{1}$$

or, alternatively,

$$\epsilon_{i-1} - 2\epsilon_i + \epsilon_{i+1} = 4\pi e^2 d n_i. \tag{2}$$

We include the possible effects of a finite dielectric constant, $\epsilon_0$, into the definition of the electrostatic charge, $e^2$.

### B. Linear response approximation

We analyze the system within the Hartree approximation, and we assume that the induced charge can be well approximated by using linear response theory (random phase approximation).

The induced electron density can be written, using linear response theory, as

$$n_i = \sum_j \chi_{i,j}\epsilon_j, \tag{3}$$

where $\chi_{i,j}$ is a static susceptibility which describes the charge density induced at layer $i$ when the potential at layer $j$ is $\epsilon_j$, and the sum runs over all layers. The calculation of these susceptibilities is given by diagrams like the one shown in Fig. 2. Their value is

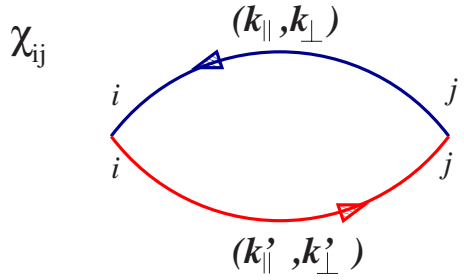


FIG. 2. (Color online) Charge susceptibility required in order to calculate the induced charge.

$$\chi_{i,j} = \sum_{\tilde{\mathbf{k}}_\parallel,\tilde{\mathbf{k}}'_\parallel,k_\perp,k'_\perp} \frac{\alpha_i^{\tilde{\mathbf{k}}_\parallel,k_\perp\,*}\alpha_i^{\tilde{\mathbf{k}}'_\parallel,k'_\perp\,*}\alpha_j^{\tilde{\mathbf{k}}_\parallel,k_\perp}\alpha_j^{\tilde{\mathbf{k}}'_\parallel,k'_\perp}}{\epsilon_{\tilde{\mathbf{k}}_\parallel,k_\perp} - \epsilon_{\tilde{\mathbf{k}}'_\parallel,k'_\perp}}, \tag{4}$$

where the intermediate empty and occupied states are labelled by their moments, $\tilde{\mathbf{k}}_\parallel,k_\perp,\tilde{\mathbf{k}}_\parallel,k'_\perp$, and $i$ and $j$ are layer indices. The quantities $\alpha_i^{\tilde{\mathbf{k}}_\parallel,k_\perp}$, $\alpha_j^{\tilde{\mathbf{k}}_\parallel,k_\perp}$, $\alpha_i^{\tilde{\mathbf{k}}'_\parallel,k'_\perp}$, and $\alpha_j^{\tilde{\mathbf{k}}'_\parallel,k'_\perp}$ in Eq. (4) are the amplitudes of the wave functions on layers $i$ and $j$, respectively. We will only consider charge distributions which are homogeneous in the directions parallel to the layers, so that the parallel momentum transfer in the diagram in Fig. 2 vanishes, $\tilde{\mathbf{q}}=\tilde{\mathbf{k}}_\parallel-\tilde{\mathbf{k}}'_\parallel=0$.

### C. Electronic structure

We describe the electronic levels of the graphene stack by means of a tight-binding model using the $\pi$ orbitals at each C atom. We consider a hopping between orbitals in atoms which are nearest neighbors within a given layer, $t=2.7$ eV, and a hopping between atoms in adjacent layers which are also nearest neighbors, $t_\perp=0.3$ eV. We study mostly the Bernal stacking, so that the hopping term connects one-half of the orbitals in a given layer with one-half of the orbitals in the two nearest layers. At long wavelengths and near half-filling the in-plane dispersion is well approximated by the continuum Dirac equation, described in terms of the Fermi velocity, $v_F=3ta/2$, where $a=1.4$ Å is the distance between carbon atoms. Details of the model, and of the band structure, for stacks with a different number of layers and stacking order are given in Ref. 18.

The system has translational invariance in the direction parallel to the layers, so that the parallel momentum, $\tilde{\mathbf{k}}_\parallel \equiv (k_x,k_y)$ is conserved. If the stack is infinite, the momentum normal to the layers, $k_\perp$, is also conserved.

In an infinite stack with only nearest-neighbor coupling between layers, all layers are equivalent (in general, a description of the Bernal stacking requires two inequivalent layers). Then, the Hamiltonian for each momentum decouples in a set of $2\times 2$ matrices, whose entries correspond to Bloch states defined in the two inequivalent sublattices of each layer. For a given corner of the Brillouin zone, the Hamiltonian can be written as

$$\mathcal{H}_{\tilde{\mathbf{k}}_\parallel,k_\perp} \equiv \begin{pmatrix} 2t_\perp \cos(k_\perp d) & v_F(k_x+ik_y) \\ v_F(k_x-ik_y) & 0 \end{pmatrix}. \tag{5}$$

The diagonal terms in Eq. (5) are determined by the interlayer hopping, so that $\mathcal{H}_{22}=0$, as one of the sublattices is

decoupled from the neighboring layers. The Hamiltonian in Eq. (5) reduces to the Dirac equation for $t_\perp = 0$.

The low-energy eigenenergies can be approximated as

$$\epsilon_{\tilde{\mathbf{k}}_\parallel k_\perp} \approx \pm \frac{v_F^2 |\tilde{\mathbf{k}}_\parallel|^2}{2t_\perp \cos(k_\perp d)}. \tag{6}$$

This approximation fails for $k_\perp d \sim \pi/2$, where the bands show a linear dependence on $\tilde{\mathbf{k}}_\parallel$.

The allowed momenta in a finite stack with $N$ layers are quantized, $k_\perp^n = (n\pi)/[d(N+1)]$.[18] In addition, the amplitude of the wave functions goes to zero as $\sin(ik_\perp c)$ at layer $i$ from the surface. The electronic wave functions in a finite stack are described in Appendix A.

### D. Calculation of the charge susceptibility

The response of the electrons at both inequivalent corners of the Brillouin zone is the same, so that we need to calculate the polarizability at one $K$ point.

The charge susceptibility includes contributions from transitions between the valence and conduction bands, interband transitions, and transitions within the conduction band, intraband transitions, as schematically depicted in Fig. 3.

We consider first the interband transitions, involving an occupied state in the valence band and an empty state in the conduction band. We neglect the contribution from the states with $k_\perp d \sim \pi/2$, and we use the approximate dispersion relation given in Eq. (6). Then, the susceptibilities in Eq. (4)

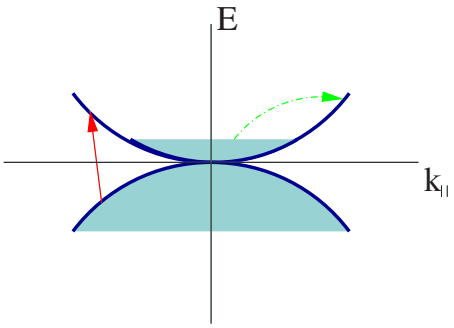


FIG. 3. (Color online) Sketch of the interband and intraband transitions whose separate contributions to the charge susceptibility are analyzed in the text.

can be written as an integral over $\tilde{\mathbf{k}}_\parallel$, $k_\perp$, and $k'_\perp$. The electronic states in a semi-infinite stack can also be characterized by a perpendicular momentum, $k_\perp$, although the corresponding wave functions are no longer running waves. Near the surface of a semi-infinite stack, the amplitudes in eq. (4) are

$$\alpha_i^{\tilde{\mathbf{k}}_\parallel, k_\perp} = C \sin(ik_\perp d), \tag{7}$$

where $C$ is a normalization constant. Note that, although one needs in principle to define the amplitude as a two component spinor in each layer, the low-energy states considered here, Eq. (6), have vanishing amplitude on the sublattice connected by the interlayer hopping $t_\perp$.[18]

Using Eq. (7), we finally obtain

$$\chi_{ij}^{\text{inter}} \approx \frac{8}{\pi^3} \frac{t_\perp}{v_F^2} \int_{-\pi/2}^{\pi/2} d\phi \int_{\pi/2}^{(3\pi)/2} d\phi' \frac{\sin(i\phi)\sin(j\phi)\sin(i\phi')\sin(j\phi')\cos(\phi)\cos(\phi')}{[\cos(\phi)+\cos(\phi')]} \int_0^{k_c} \frac{dk}{k} = \frac{4}{\pi} \frac{t_\perp}{v_F^2} \tilde{\chi}_{ij} \ln\left(\frac{t_\perp}{\epsilon_0}\right), \tag{8}$$

where $\epsilon_0$ is a low-energy cutoff to be specified later, and we write $\phi = k_\perp d$ and $\phi' = k'_\perp d$. In a finite stack, these integrals over $k_\perp$ and $k'_\perp$ must be replaced by sums over the quantized momenta, see Sec. III B. The prefactor $\tilde{\chi}_{ij}^{\text{inter}}$ in Eq. (8) is defined as

$$\tilde{\chi}_{ij}^{\text{inter}} = \frac{1}{\pi^2} \int_{-\pi/2}^{\pi/2} d\phi \int_{\pi/2}^{3\pi/2} d\phi' \times \frac{\sin(i\phi)\sin(j\phi)\sin(i\phi')\sin(j\phi')\cos(\phi)\cos(\phi')}{\cos(\phi)-\cos(\phi')}. \tag{9}$$

The values of $\chi_{ij}^{\text{inter}}$ near the boundary of the stack are plotted in Fig. 4. The limiting bulk values

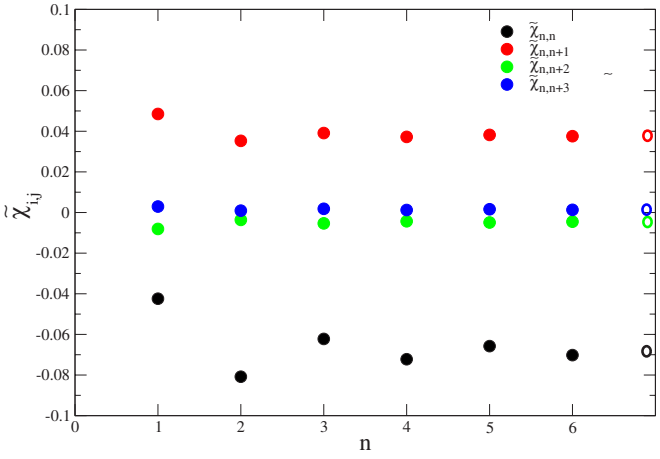


FIG. 4. (Color online) Value of the prefactor in the susceptibilities near the boundary of a stack of graphene planes, see Eq. (8). The corresponding bulk values are plotted as open circles on the right-hand side.

$$\tilde{\chi}^{\text{inter}}_{m+n,m} = \tilde{\chi}^{\text{inter}}_{n} = \frac{1}{4\pi^2}\int_{-\pi/2}^{\pi/2} d\phi \int_{\pi/2}^{3\pi/2} d\phi' \frac{\cos[n(\phi-\phi')]\cos(\phi)\cos(\phi')}{\cos(\phi)-\cos(\phi')} \tag{10}$$

are also shown.

## III. RESULTS

### A. Undoped semi-infinite stack

In a semi-infinite stack, sufficiently far from the surface, so that the susceptibilities $\chi_{ij}$ have converged towards their bulk values, Eqs. (2) and (3) admit the solution

$$\epsilon_i = \epsilon_0 e^{-\kappa},$$

$$n_i = n_0 e^{-\kappa} \tag{11}$$

with

$$e^{\kappa} + e^{-\kappa} - 2 = 4\pi e^2 d \sum_{n=-\infty}^{\infty} e^{n\kappa} \chi_n^{\text{inter}} = \frac{8e^2 dt_\perp}{\pi v_F^2} \ln\left(\frac{t_\perp}{\epsilon_0}\right) \times \left\{ \frac{1+\cosh(\kappa)}{2\sinh(\kappa/2)} \arctan\left[\sinh\left(\frac{\kappa}{2}\right)\right] - 1 \right\}. \tag{12}$$

Details of the steps involved in the derivation of Eq. (12) are given in Appendix B.

In metallic systems and for $\kappa \to 1$, the right-hand side in Eq. (12) is equal to $\lim_{k_\perp \to 0} \chi(k_\perp, \tilde{\mathbf{k}}_\parallel = 0) = D(\epsilon_F)$, where $D(\epsilon_F)$ is the density of states at the Fermi level in a given layer. Using this result, we obtain the Thomas-Fermi approximation, $\kappa^2 = 4\pi e^2 d D(\epsilon_F)$ in the limit $\kappa \to 0$.

For the model of undoped graphite studied here, the right-hand side of Eq. (12) vanishes as $\kappa \to 0$, and ordinary screening does not take place.

The contribution of the interband transitions to the charge susceptibility is not enough to give a finite charge compressibility at long wavelengths, leading to a behavior reminiscent of that of an insulator. Note that, at zero doping, the transitions between occupied and empty states in the limit $\phi - \phi' \to 0$ require a finite energy of order $t_\perp \cos(\phi)$, except for $\phi \approx \phi' \approx \pi/2$. These transitions have vanishing weight in the integral which gives the charge compressibility (see Fig. 5). Hence, the charge susceptibility tends to zero at zero energy and $k_\perp d \to 0$.

Note that, on the other hand, the staggered spin and charge susceptibilities, $k_\perp d \neq 0$, diverge logarithmically at $\omega \to 0$.[21] This divergence is maximal for $k_\perp d = \pi$.

Equation (12) admits only solutions with $\kappa > 0$, if

$$\frac{4e^2 dt_\perp}{\pi v_F^2} \ln\left(\frac{t_\perp}{\epsilon_0}\right) \geq 6. \tag{13}$$

The scale $\epsilon_0$ in Eq. (8) determines the region where the model gives a valid description of a graphene stack. At zero temperature, it will be determined by interlayer hoppings not considered here, disorder, and lifetime broadening due to interaction effects. At finite temperatures, the logarithmic divergence in Eq. (8) is cutoff by thermal interband excitations, so that $\epsilon_0 \approx T$. Hence, the screening properties of the model depend on temperature.

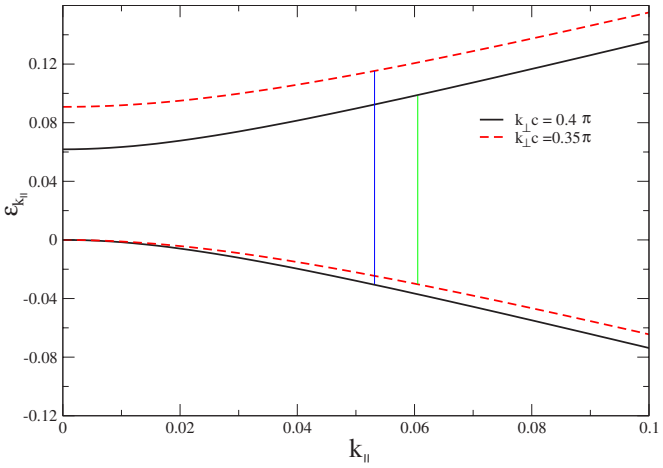


FIG. 5. (Color online) Transitions between the valence and conduction bands states for $(k_\perp - k'_\perp)c = 0.05\pi$ and $k_\perp c = 0.4\pi$. The parameters used are $v_F = 1$ and $t_\perp = 0.1$.

At the surface, the screening by interband transitions is modified, as the relative strength of the different subbands, as a function of $k_\perp$, is modified. The contribution to the real space matrix elements of the susceptibility are given by

$$\chi_{ij}^{\text{intra}} = \frac{8t_\perp}{\pi^2 v_F^2} \int_{-\pi/2}^{\pi/2} d\phi \sin(\phi i)^2 \sin(\phi j)^2 \cos(\phi). \tag{14}$$

At finite dopings the density of states of each graphene plane in the model studied here is

$$D(\epsilon_F) = \frac{4t_\perp}{\pi^2 v_F^2} \tag{15}$$

independent of the carrier concentration. Intraband transitions modify the charge susceptibility as $k_\perp \to 0$. The charge compressibility becomes finite, leading to a bulk screening length,

$$\kappa^2 = \frac{16e^2 dt_\perp}{\pi v_F^2}. \tag{16}$$

In the following, we use the parameters

$$\frac{e^2}{v_F} \approx 1,$$

$$\frac{t_\perp d}{v_F} \approx \frac{1}{5}. \tag{17}$$

Using these values, Eq. (16) gives a screening length due to bulk intraband transitions of about $N \sim 2$ layers. The screening at the surface, however, is modified and reduced, as shown in Eq. (14).

Numerical results, including the full dependence on the position of $\tilde{\chi}_{m,m+n}$ are shown in Fig. 6. We have chosen the

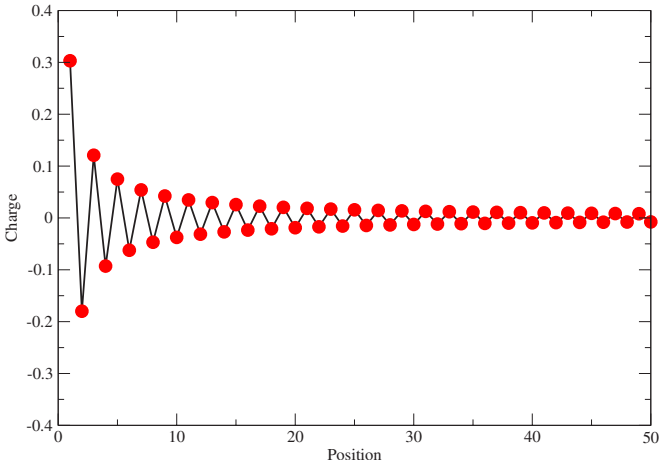


FIG. 6. (Color online) Charge at the surface of a semi-infinite stack, normalized to one. Only interband transitions are included in the calculation.

parameter $\epsilon_0$ such that $\ln(t_\perp/\epsilon_0)=6$. The charge oscillates with every second layer. This result is consistent with the logarithmic divergence of the charge and spin susceptibility for $k_\perp d=\pi$. The induced charge is reduced to less than 10% of the charge in the surface layer in about $N\sim 3-5$ layers.

### B. Finite stacks

Equations (2) and (3) can be solved in a straightforward way for a system with a few layers. The discrete equivalent to the reduced susceptibilities in Eq. (9) can be defined as

$$\tilde{\chi}_{ij}^{\text{inter}} = \sum_{n=1}^{N}\sum_{n'=1}^{N} \sin(k_\perp^n di)\sin(k_\perp^n dj)\sin(k_\perp^{n'} di)\sin(k_\perp^{n'} dj) \times \frac{\cos(k_\perp^n d)\cos(k_\perp^{n'} d)}{C_{k_\perp^n} C_{k_\perp^{n'}}[\cos(k_\perp^n d)-\cos(k_\perp^{n'} d)]} a, \tag{18}$$

where $C_{k_\perp^n}$ is a normalization constant,

$$C_{k_\perp^n} = \sum_{l=1}^{N} \sin^2(k_\perp^n cl). \tag{19}$$

A finite bilayer can be charged, so that the Fermi energy does not need to lie exactly between the valence and conduction bands. Then, we must add to the susceptibility a contribution from intraband transitions at $\tilde{\mathbf{k}}_\parallel \to 0$. The contribution of each subband is determined by its contribution to the total density of states, and it is independent of the position of the Fermi level. Hence, intraband transitions lead to

$$\chi_{ij}^{\text{intra}} = \frac{2t_\perp}{\pi^2 v_F^2}\sum_n \frac{\sin^2(k_\perp^n di)\sin^2(k_\perp^n dj)|\cos(k_\perp^n d)|}{C_{k_\perp^n}^2}. \tag{20}$$

The charge distribution is given by the equations

$$\epsilon_i = \epsilon_{i-1} + 4\pi e^2 d\sum_{k=1}^{i-1} n_k,$$

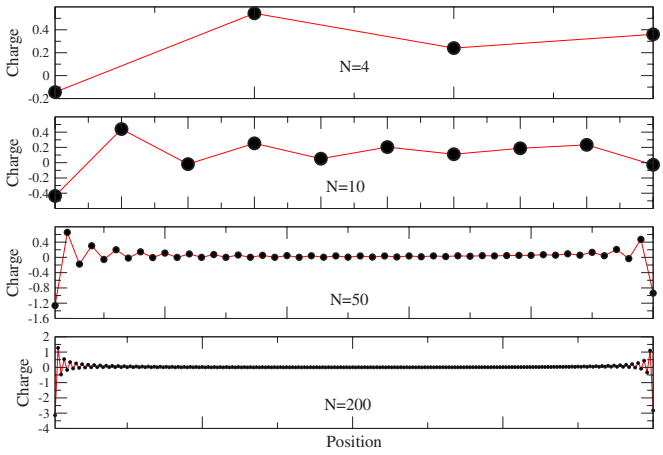


FIG. 7. (Color online) Charge distribution in systems with 4, 10, 50, and 200 graphene layers, normalized to one.

$$n_i = n_0 + \sum_{j=1}^{N} (\chi_{ij}^{\text{inter}} + \chi_{ij}^{\text{intra}})\epsilon_j, \tag{21}$$

where $n_0$ is a constant which fixes the total density, in turn determined by the applied field between the gate and the stack.

The diagonal intraband susceptibilities near the surface of a semi-infinite stack satisfy

$$\tilde{\chi}_{nn}^{\text{intra}} \propto \int_{-\pi/2}^{\pi/2} d\phi \sin^4(n\phi)\cos(\phi) = -\frac{1}{4(16n^2-1)} + \frac{(-1)^n}{2n^2-1} + \frac{3}{4} \tag{22}$$

showing even-odd oscillations as a function of the distance to the surface, $n$, as well as a slow convergence to the bulk limit, $n\to\infty$.

If we neglect the intraband susceptibility, we find for a bilayer,

$$\epsilon_1 - \epsilon_2 = \frac{2\pi e^2 d n_0}{1-2\pi e^2 d(\chi_{11}-\chi_{12})}, \tag{23}$$

where $n$ is the total carrier density, and $\chi_{11}$ and $\chi_{12}$ are the bilayer interband susceptibilities, defined using Eqs. (18) and (8). By choosing the low-energy cutoff, $\epsilon_0$, such that $\epsilon_0=\epsilon_F=(\pi v_F^2 n_0)/t_\perp$, we recover the results in Ref. 20 to lowest order in $n_0$.

Examples of the charge distribution in doped systems with a different number of layers are shown in Fig. 7. We find the following:

(i) The charge distribution is rather homogeneous in narrow stacks, and it becomes concentrated at the surfaces for stacks wider than the screening length.

(ii) There are oscillations as a function of the distance to the surface in wide stacks, as in the case of a semi-infinite stack. These oscillations can lead to charge with different sign in neighboring layers.

## IV. CONCLUSIONS

We have calculated the charge distribution in stacks of graphene layers in an applied field. We describe the electronic structure by a tight-binding model for the $\pi$ orbitals, which includes hopping between sites which are nearest neighbors in adjacent layers. The self-consistent electrostatic potential is obtained assuming linear response theory, so that our approximations amount to the random phase approximation.

The electronic structure of these systems shows a valence band and conduction band with parabolic dispersion as a function of the parallel momentum, for all values of the perpendicular momentum. These bands touch at zero energy, which defines the chemical potential in the undoped case. Finite and infinite stacks are gapless.

The charge susceptibility can be written as a sum of intraband and interband contributions. In a clean, neutral system only interband transitions contribute. In this case, an infinite stack of layers shows nonmetallic screening, as the long-wavelength charge susceptibility vanishes.

The charge susceptibility for finite momenta perpendicular to the layers shows a logarithmic divergence at low energies. This divergence is maximal for a wave vector inversely proportional to the distance between the layers, leading to charge oscillations. In addition, the logarithmic divergence at finite wave vectors implies that the screening properties of undoped systems can show a dependence on the frequency at which they are probed, or on temperature.

The charge distribution induced at a surface can be extended over many layers, and it shows a decaying modulation with a period equal to the distance between the layers.

In doped samples, the long-wavelength charge polarizability is finite, and it is dominated by intraband transitions. We find that an external field is screened within three-to-five layers from the surface. The screening length is independent of carrier concentration. The interband transitions lead to oscillations in the induced charge, as in the undoped case. As these fluctuations depend logarithmically on a low-energy cutoff, they can also show a dependence on temperature or frequency.

The screening length in doped stacks obtained here depends on the values of the parameters given in (17). Their bulk values are not known with precision,[22] and it is possible that some of them, like the effective electric charge or the interlayer hopping, change near an interface. Hence, the value of three-to-four layers over which the charge is delocalized in doped samples is only approximate.

Our calculation does not take into account effects such as next-nearest-neighbor hoppings, disorder, or deviations from the linear response. The existence of other hoppings, or disorder, will define a low-energy scale below which the results will no longer be valid.

Deviations from linear response theory depend on the strength of the induced electrostatic potential with respect to the parameters which define the band structure, the smaller of which is the interlayer hopping, $t_\perp$, which we have assumed to be $t_\perp \sim 0.1-0.3$ eV. Typical differences in electrostatic potentials between adjacent layers are given by $\epsilon_i - \epsilon_{i-1} \approx e^2 dn$, where $n$ is the induced charge per unit area. For $n \sim 10^{11}-10^{12}$ cm$^{-2}$, we obtain $\epsilon_i - \epsilon_{i-1} \sim 10^{-3}-10^{-2}$ eV, so that the assumption of linear response is probably valid. Finally, we have only studied the Bernal stacking, $1212\cdots$. Regions of rhombohedral stacking reduce the density of states near the Fermi level,[18] and they will decrease the screening in the system.

It is interesting to consider the similarities and differences of this work with the related calculation in Ref. 17. In this reference, it was assumed that a low-density two-dimensional electron gas existed in each layer, and that the electrons could not move between different layers. This approximation is equivalent to consider only the diagonal susceptibility, $\chi_{nn}$, in Eq. (8). For the 2DEG, only intraband transitions exist, leading to $\chi_{nn} = D(\epsilon_F) = n_v[m^*/(\pi\hbar^2)]$, where $n_v$ is the number of valleys. This assumption leads to metallic screening, with a decay of the electrostatic potential into the bulk, Eq. (12), given by $\kappa^2 \approx (e^2 d n_v m^*)/(\pi\hbar^2)$. In our case, the existence of a finite density of states near the Fermi level is a consequence of the finite interlayer hopping, $t_\perp$, as the electronic structure reduces to a stack of decoupled Dirac equations in the absence of hopping. The charge oscillations near a surface are directly related to the quantum coherence between stacks induced by the interlayer hopping. Hence, they cannot be obtained in the model used in Ref. 17.

## ACKNOWLEDGMENTS

The author is thankful to A. Castro Neto for many helpful discussions. Financial support from the Ministerio de Educación y Ciencia (Spain) through Grant No. FIS2005-05478-C02-01, the European Union, through Contract No. 12881, and the program CITECNOMIK (C. A. Madrid), Contract No. CM2006-S-0505-ESP-0337 is gratefully acknowledged.

## APPENDIX A: ELECTRONIC WAVE FUNCTIONS IN FINITE STACKS

We define the amplitude of the wave function with parallel momentum $\tilde{\mathbf{k}}_\parallel$, perpendicular momentum $k_\perp^n$ at layer $M$ as a two-component spinor,

$$\Psi_{\tilde{\mathbf{k}}_\parallel, k_\perp^n, M} \equiv \begin{pmatrix} \alpha_{\tilde{\mathbf{k}}_\parallel, k_\perp^n, M} \\ \beta_{\tilde{\mathbf{k}}_\parallel, k_\perp^n, M} \end{pmatrix}, \tag{A1}$$

where $\alpha_{\tilde{\mathbf{k}}_\parallel, k_\perp^n, M}$ and $\beta_{\tilde{\mathbf{k}}_\parallel, k_\perp^n, M}$ refer to the amplitudes on the $A$ sublattice, whose atoms in different layers are nearest neighbors, and the $B$ sublattice, whose atoms in different layers are not connected. In order to satisfy the open boundary conditions at the surfaces of the stack, these amplitudes must be of the form

$$\begin{pmatrix} \alpha_{\tilde{\mathbf{k}}_\parallel, k_\perp^n, M} \\ \beta_{\tilde{\mathbf{k}}_\parallel, k_\perp^n, M} \end{pmatrix} \equiv \begin{pmatrix} \alpha_{\tilde{\mathbf{k}}_\parallel, k_\perp^n} \\ \beta_{\tilde{\mathbf{k}}_\parallel, k_\perp^n} \end{pmatrix} \sin(k_\perp^n c M) \tag{A2}$$

and

$$\begin{pmatrix} 2t_\perp \cos(k_\perp^n c) & v_F(k_x + ik_y) \\ v_F(k_x - k_y) & 0 \end{pmatrix} \begin{pmatrix} \alpha_{\tilde{\mathbf{k}}_\parallel, k_\perp^n} \\ \beta_{\tilde{\mathbf{k}}_\parallel, k_\perp^n} \end{pmatrix} = \epsilon_{\tilde{\mathbf{k}}_\parallel, k_\perp} \begin{pmatrix} \alpha_{\tilde{\mathbf{k}}_\parallel, k_\perp^n} \\ \beta_{\tilde{\mathbf{k}}_\parallel, k_\perp^n} \end{pmatrix}. \tag{A3}$$

The low-energy eigenvalues, $|\epsilon_{\tilde{\mathbf{k}}_\parallel, k_\perp^n}| \ll t_\perp$ are given by

$$\epsilon_{\tilde{\mathbf{k}}_\parallel, k_\perp^n} = \pm t_\perp \cos(k_\perp^n c) \mp \sqrt{t_\perp^2 \cos^2(k_\perp c) + v_F^2 |\tilde{\mathbf{k}}_\parallel|^2}$$

$$\approx \mp \frac{v_F^2 |\tilde{\mathbf{k}}_\parallel|^2}{2t_\perp \cos(k_\perp^n c)} \tag{A4}$$

within this low-energy approximation, Eq. (A3) implies that

$$\begin{pmatrix} \alpha_{\tilde{\mathbf{k}}_\parallel, k_\perp^n} \\ \beta_{\tilde{\mathbf{k}}_\parallel, k_\perp^n} \end{pmatrix} \approx \begin{pmatrix} C_{k_\perp^n}^{1/2} \\ 0 \end{pmatrix}, \tag{A5}$$

where $C_{k_\perp^n}^{1/2}$ is a normalization constant.

## APPENDIX B: CALCULATION OF THE BULK SUSCEPTIBILITY

We derive the right-hand side of Eq. (12) using the expressions in Eq. (10). The dependence on the layer index $n$ in Eq. (10) is through the factor $\cos[n(\phi - \phi')]$. In order to regularize the summations over $n$, we add a small decaying factor, $\epsilon$,

$$\cos[n(\phi - \phi')] \to e^{-\epsilon|n|} \cos[n(\phi - \phi')]. \tag{B1}$$

For $\kappa = 0$ in Eq. (12) the $n$-dependent part of the sum gives

$$\sum_{n=-\infty}^{\infty} e^{-\epsilon|n|} e^{in(\phi_0 + \phi - \phi')} = \frac{\sinh(\epsilon)}{\cosh(\epsilon) - \cos(\phi_0 + \phi - \phi')} \overset{\epsilon}{\to} 2\pi\delta(\phi_0 + \phi - \phi'), \tag{B2}$$

where, for convenience, we have also included a shift, $\phi_0$. Using this result, we also obtain

$$\mathcal{F}(\phi_0) = \int_{-\pi/2}^{\pi/2} d\phi \int_{\pi/2}^{3\pi/2} d\phi' \sum_{n=-\infty}^{\infty} \cos[n(\phi_0 + \phi - \phi')] \times \frac{\cos(\phi)\cos(\phi')}{\cos(\phi) - \cos(\phi')} \int_{-\pi/2}^{\pi/2} d\phi \frac{\cos(\phi)\cos(\phi_0 + \phi)}{\cos(\phi_0 + \phi) - \cos(\phi)}$$

$$= \frac{1 + \cos(\phi_0)}{4 \sin(\phi_0/2)} \ln\left(\frac{1 + \sin(\phi_0/2)}{1 - \sin(\phi_0/2)}\right) - 1. \tag{B3}$$

The summation for $\kappa \neq 0$ in Eq. (12) is formally equivalent to the replacement $\phi_0 \to i\kappa$. Making this substitution, we find

$$\mathcal{F}(i\kappa) = \frac{1 + \cosh(\kappa)}{2 \sinh(\kappa/2)} \arctan\left[\sinh\left(\frac{\kappa}{2}\right)\right] - 1. \tag{B4}$$

For $\kappa \to 0$ we find

$$\mathcal{F}(i\kappa) \approx \frac{\kappa^2}{6} + \frac{\kappa^4}{180} + \cdots. \tag{B5}$$


[1] C. Berger *et al.*, J. Phys. Chem. B **108**, 19912 (2004).
[2] K. S. Novoselov, D. Jiang, F. Schedin, T. J. Booth, V. V. Khotkevich, S. V. Morozov, and A. K. Geim, Proc. Natl. Acad. Sci. U.S.A. **102**, 10451 (2005).
[3] K. S. Novoselov, A. K. Geim, S. V. Morozov, D. Jiang, M. I. Katsnelson, I. V. Grigorieva, S. V. Dubonos, and A. A. Firsov, Nature (London) **438**, 197 (2005).
[4] Y. Zhang, Y.-W. Tan, H. L. Stormer, and P. Kim, Nature (London) **438**, 201 (2005).
[5] Y. Zhang, J. P. Small, M. E. S. Amori, and P. Kim, Phys. Rev. Lett. **94**, 176803 (2005).
[6] J. S. Bunch, Y. Yaish, M. Brink, K. Bolotin, and P. L. McEuen, Nano Lett. **5**, 2887 (2005).
[7] Y. Zhang, J. P. Small, W. V. Pontius, and P. Kim, Appl. Phys. Lett. **86**, 073104 (2005).
[8] C. Berger *et al.*, Science **312**, 1191 (2006).
[9] S. V. Morozov, K. S. Novoselov, F. Schedin, D. Jiang, A. A. Firsov, and A. K. Geim, Phys. Rev. B **72**, 201401(R) (2005).
[10] Y. Lu, M. Muñoz, C. S. Steplecaru, C. Hao, M. Bai, N. García, K. Schindler, and P. Esquinazi, Phys. Rev. Lett. **97**, 076805 (2006).
[11] J. Nilsson, A. H. Castro Neto, F. Guinea, and N. M. R. Peres, Phys. Rev. Lett. **97**, 266801 (2006).
[12] A. K. Geim and K. S. Novoselov, Nat. Mater. **6**, 183 (2007).
[13] J. González, F. Guinea, and M. A. H. Vozmediano, Nucl. Phys. B: Field Theory Stat. Syst. **485[FS]**, 694 (1997).
[14] J. González, F. Guinea, and M. A. H. Vozmediano, Phys. Rev. B **59**, R2474 (1999).
[15] J. González, F. Guinea, and M. A. H. Vozmediano, Phys. Rev. B **63**, 134421 (2001).
[16] N. M. R. Peres, F. Guinea, and A. H. Castro Neto, Phys. Rev. B **73**, 125411 (2006).
[17] P. B. Visscher and L. M. Falicov, Phys. Rev. B **3**, 2541 (1971).
[18] F. Guinea, A. H. Castro Neto, and N. M. R. Peres, Phys. Rev. B **73**, 245426 (2006).
[19] E. McCann and V. I. Fal'ko, Phys. Rev. Lett. **96**, 086805 (2006).
[20] E. McCann, Phys. Rev. B **74**, 161403(R) (2006).
[21] J. Nilsson, A. H. Castro Neto, N. M. R. Peres, and F. Guinea, Phys. Rev. B **73**, 214418 (2006b).
[22] N. B. Brandt, S. M. Chudinov, and Y. G. Ponomarev, in *Modern Problems in Condensed Matter Sciences*, edited by V. M. Agranovich and A. A. Maradudin (North-Holland, Amsterdam, 1988), Vol. 20.1.